A thermodynamically consistent poro-visco-elastic model of the Extracellular Matrix

Giulia Laura Celora

Mathematical Institute, University of Oxford

Abstract.

1 Introduction

There are several studies supporting the central role of mechanical stimuli in tissue morphogenesis and homeostasis [5,43]. In tissues, cells are mainly surrounded by extracellular matrix (ECM), a soft porous media made up of networks of polymer chains and charged proteins which is mixed with interstitial fluid. *In vitro* studies have shown that ECM rigidity and shear stresses due to the flow of interstitial fluid can promote malignant phenotypes in a population of initially normal cells, impact on cell proliferation and differentiation [9]. Further experiments have shown that tumour development is often associated with a stiffening of the tissue compared to the surrounding healthy one [41]. This causes cells to be exposed to higher compressive stresses and the collapse of blood vessels, thus impeding the diffusion of substances in the extra-cellular environment. Hence, numerous therapies are less effective [48]. Based on such evidence, it is now widely accepted that, unlike originally thought, biological process are not simply regulated by biochemical signals but by the complex interplay of mechanical and chemical stimuli.

Given the different physical nature and scale of phenomena involved, coupling micro-environment and cell behaviours is a problem of high complexity. This requires understanding processes occurring at different temporal and spatial scales and how they interplay to determine the macroscopic behaviour of a tissue, whether healthy or damaged. Despite experiments probing the micro-scale are nowadays possible, these are usually limited to controlled environment in contrast to *in vivo* conditions. On the other hand, macro-scale measurements are easier to gather, but give only information on average properties, which do not correspond to what cell experience. Hence, in order to manipulate the cell environment, we need quantitative models able to link this two scales. Having such knowledge, this could led to the development of novel therapies and completely change our approach to drug design. In order for this to be possible, alongside experiments, it is necessary to develop a theoretical framework able to capture both the biology and physics involved and which is consistent with the known universal laws of Nature [29].

With the development of new experimental techniques such as Atomic Force Microscopy (AFM), the local mechanical properties of a material can be measured with nanometre precision [27]. When tested at this scale, soft tissues and the ECM in particular have been found to be visco-elastic [33], independently from the presence of the interstitial fluid. Where purely elastic solids can only store energy when deformed, viscoelastic materials instead exhibit a time-dependent response to mechanical deformation as part of the energy is dissipated in the deformation process. This is associated with entropic favourable changes in the conformation of the ECM network itself. While a large amount of literature focuses on the poro-elastic properties of ECM, it remains unclear the role of viscosity in determining cell behaviour. However, the recent efforts to develop synthetic ECM, i.e. hydrogels, with tunable viscoelasticity, have now opened new research opportunities [12].

As discussed in Section 2, from our point of view the ECM behaves as a polyelectrolyte gel [47,48], i.e. hydrogels with charged group. Besides being largely present in the natural world, synthetic polyelectrolytes are currently employed for a wide range of applications, such as drug delivery, biomedical devices, scaffolds for tissue engineering and soft robotics [8,13,14,34]. Hence, there has been a growing interest in the soft matter community in understanding their behaviour and translating it into mathematical models. In particular, research has been focusing on the phenomena of swelling, i.e. large deformation due to absorption of water, and the diffusion transport and release of solution [17,18,25,49]. However, theoretical studies of viscoelastic soft materials remain limited. Most of the literature has been proposing poro-elastic models, which account for the dissipation of energy due to the transport of solutions but neglect the visco-elastic response of the material itself [10]. While this assumption might be valid for certain applications, the empirical studies previously mentioned highlight the need of including this component in the study of living tissues.

As discussed in [27], there are spatial and time scales which allow to study the two independently. On one hand, nanoscale rheological testing with AFM give us information on the visco-elastic properties of the sample. For sufficiently small beads, the length scale considered in the experiment is so short that poroelastic relaxation is almost instantaneous and thus negligible. Different 1D rheological model are usually applied to fit experimental measurement: the most common for tissue and hydrogels is the *Standard Linear Solid* model, see Figure 1, to fit the experimental data [10,27]. The poro-elastic behaviour can instead be characterized by standard creep-relaxation test on whole sample. In this case, Darcy's law is usually applied to estimate the hydraulic conductivity and thus characterise the transport of fluid in the material [38,27]. Despite having a good understanding of the two phenomena independently, there has been little attention to investigating how to two couple.

Our works aims to develop a continuum mathematical model of the extracellular matrix which is consistent with the laws of thermodynamics, which accounts for its poro-visco-elastic properties and the coupling of mechanical, transport and electrical phenomena. Nonetheless, our results are more widely applicable to the

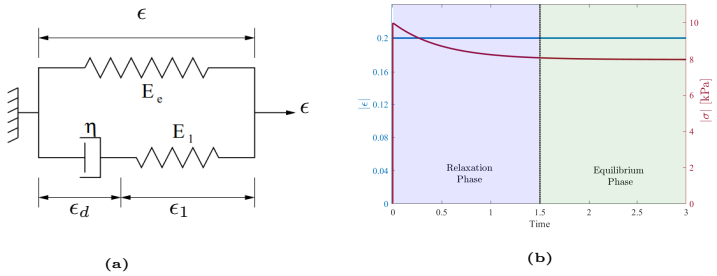

$$\begin{cases} \sigma = (E_e + E_1)\epsilon - E_1\epsilon_d \\ \dot{\epsilon}_d + \frac{E_1}{\nu}\epsilon_d = \frac{E_1}{\nu}\epsilon \end{cases} \tag{SLS}$$

Fig. 1: 1D Standard Linear Solid. (a) Rheological Model; (b) Standard Response to a compression test. (1) Differential Equation for the Standard Linear Solid model in the 1D case.

study of polyelectrolyte gels. At our present knowledge, there is no previous work in the literature capturing all these aspects in a thermodynamic consistent model. In [47,48] Xue et al. develop a nonlinear poroelastic theory for ECM, which couples all three physical phenomena but does not include viscous dissipation. In [21], the authors couple mechano-electrophysiological effects including the viscous dissipation but neglect transport; Caccavo et al. [10] propose a poro-viscoelastic model for neutral hydrogel, thus excluding electrical effects. Following these previous work, we will derive our model in the framework of linear non-equilibrium thermodynamics [29] accounting for multiple phases.

Despite the large number of studies that have characterised the poro-elastic and visco-elastic properties of ECM independently, little is known about their combined effect. In the literature, two main constitutive models have been presented, but never rigorously compared. Instead of arbitrarily choosing one of the two, we here develop both approaches, with the aim of identifying their differences and investigating experimental result which would allow us to experimentally test which one best describes the behaviour of soft tissues.

Our work is organized as follows: in Section 2, we discuss more in details the composition of the ECM. We then present a brief overview of Classical Irreversible Thermodynamics, which focuses on the principles later used in the derivation of our model in Section 4. Common [... FOLLOWING SECTIONS TO UPDATE AS I WRITE.]

2 Composition of Extracellular Matrix.

Despite the tissue-specific nature of Extracellular Matrix (ECM), this is usually composed of a network of collagen fibrils entangled with proteoglycans (PGAs) which are covalently bonded to charged chains of glycosaminoglycans (GAGs), see Figure 2a. While collagen is mainly responsible for the mechanical behaviour of the tissue, GAGs can imbibe water, giving the extracellular matrix the ability

to swell while maintaining its structural integrity. As mentioned in the introduction, from this point of view, the ECM is a polyelectrolyte gel. As schematically illustrated in Figure 2(b), polyelectrolyte gels are 3D networks of cross-linked polymer chains that contain ionizable functional groups. When in solution the gel swells, while the functional groups dissociate into fixed charges and mobile ions in the solution. In particular, research has been focusing on the phenomena of swelling, i.e. large deformation due to absorption of water, and the diffusion transport and release of solution [17,18,25,49]. However, only a small fraction of the study published accounts for the visco-elastic properties of the polymer network.

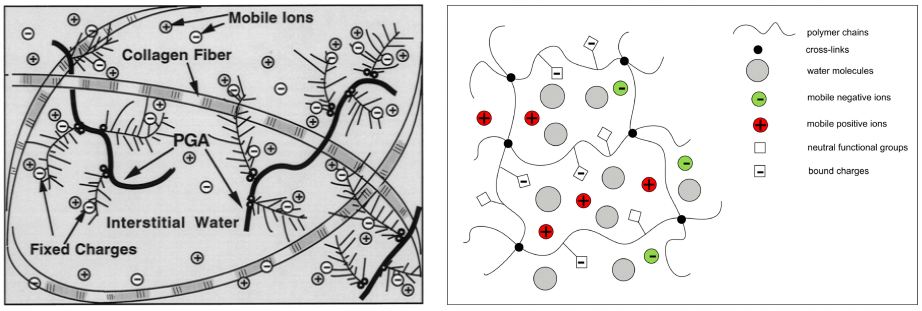

(a) (b)

Fig. 2: Analogy between ECM in soft tissue and polyelectrolytes hydrogels: (a) schematic diagram of the structure of the charged hydrated articular cartilage, reproduced from [44]; (b) an anionic polyelectrolyte gel modelled as a three-phase continuum, reproduced from [18].

As shown in Figure 2, the extracellular matrix falls into the definition of polyelectrolytes so that the knowledge acquired in the study of these materials can be transferred to soft tissues. For the purpose of this study, we will not explicitly distinguish between collagen, PGAs and GAGs. At the tissue level, this can be grouped into a single solid phase (the polymer network), whose mechanical properties are treated as the average over the different components contribution. As is common in multiphase models of tissue, we will assume that the matrix is isotropic and GAGs are evenly distributed on the network. While this is not a good approximation for tissue like cartilage, which are highly anisotropic, it does apply to the extracellular matrix found in soft tissue such as liver, brain and tumours. It is also important to point out that ECM has additional properties such as thermo-sensitivity and pH-sensitivity. However, both in living organisms and in experimental set-up temperature and pH are maintained fairly constant.

3 Non Equilibrium Thermodynamics.

While equilibrium thermodynamics can describe ideal, i.e. reversible, processes, it does not apply to real processes which are irreversible. In this cases, the change in the entropy of a system $\mathrm{d}S$ results from both the reversible exchange of energy and matter with the external environment $\mathrm{d}_e S$ and the internal dissipation of energy during the process $\mathrm{d}_i S$ [29]:

$$\mathrm{d}S = \mathrm{d}_e S + \mathrm{d}_i S, \tag{1}$$

According to the second law of thermodynamics, which applies universally to any system or any of its sub-part $\mathrm{d}_i S \geq 0$. It is important to notice that the second law allows transformations in which total change in entropy dS of the system is negative. This occurs whenever $-\mathrm{d}_e S > \mathrm{d}_i S$ and it can lead to the spontaneous formation of complex and ordered structures such as living organisms. From this point of view, life has emerged as an efficient mechanism able to increase sufficiently the entropy of its environment [36].

In this study, we will focus on isothermal processes, i.e. $T = const.$ Under this assumption, as derived by Gurtin in [23], the second law of thermodynamics is equivalent to the following *energy imbalance inequality*:

$$\frac{\mathrm{d}}{\mathrm{d}t}\left\{\int_R \psi\right\} \leq W(R) + M(R) \tag{2}$$

where R is a arbitrary control volume of the system, ψ is the Helmholtz free energy, $W(R)$ is the rate at which the environment does work on R and $M(R)$ is the inflow of mass due to transport. It is important to note that, as long as the quantities involved are well defined, the energy inequality (2) holds for any isothermal process independently of the specific physical system considered. This imposes a constraint on the form of the function ψ and its dependence on the other thermodynamic variables, such as temperature or pressure, which are used to describe the system.

Non-equilibrium thermodynamics mainly focuses on defining the form of $\mathrm{d}_i S$, which, unlike the reversible entropy production $\mathrm{d}_e S$, is not a state variable but depends on the specific transformation applied to the system. Different theories have been proposed, [29], each with its assumptions and specific domain of applicability. In our study we will focus on "Classical Irreversible Thermodynamics" (CIT) which was pioneered by Onsager [40] and Prigogine [42] in the first half of the 20th century. One the most important assumptions of this theory is the *Local Equilibrium Hypothesis*, which guarantees thermodynamic variables, including entropy, are locally well-defined, [29]. Consequently, we can introduce the entropy density $s = s(\mathbf{x}, t)$ such that:

$$S = \int_R s \,\mathrm{d}V, \qquad \mathrm{d}s = \mathrm{d}_e s + \mathrm{d}_i s, \qquad \mathrm{d}_i s > 0, \tag{3}$$

and the local entropy production:

$$\sigma \equiv \frac{\mathrm{d}_i s}{\mathrm{d}t} \geq 0. \tag{4}$$

Another central aspect of the theory is the introduction of *thermodynamic forces* [1] F_m (causes) and *thermodynamic fluxes* J_m (effects) to describe the time evolution of the system during an irreversible transformation. These are related to σ as follows:

$$\sigma = \sum_m F_m J_m \geq 0. \tag{5}$$

[1] Not to be intended in the mechanical sense

While the local equilibrium hypothesis is at the basis of most theories of non-equilibrium thermodynamics, the following two hypotheses uniquely identify CIT:

1. *Linear Relation between forces F and fluxes J*:

$$J_m = \sum_k L_{mk} F_k, \tag{6}$$

   where the constant L_{mk} are referred to as **phenomenological coefficients**;
2. *Microscopic Reversibility*: time reversibility of processes at the micro-scale.

Starting from these two principles, in his seminal paper [40] Onsager derives the well-known *Onsager Reciprocal Relation*:

$$L_{mk} = L_{km}. \tag{7}$$

If we now consider an isothermal transformation in the framework of CIT, alongside with the energy imbalance inequality, we have that the following must hold:

$$W(R) + M(R) - \frac{\mathrm{d}}{\mathrm{d}t}\left\{\int_R \psi\right\} = T \int_R \sigma \, \mathrm{d}V \,, \tag{8}$$

In the past few decades, CIT has been applied successfully to the modelling of several physical phenomena of interest for engineers, physicists and applied mathematicians. However, its validity is limited to phenomena near-equilibrium, for which a linear approximation of the flux-force relation holds. The growing interest in more complex far-from-equilibrium phenomena has pushed toward the development of a more general framework for the study of a non-equilibrium phenomena. Since this goes beyond the purpose of our study, we will not discuss it further. We do, however, highlight the law of steepest entropy ascent, which, according to Beretta [3], seems to emerge as the fourth fundamental law of nature. In the linear regime, this principle can be used to prove Onsager's reciprocal relation [2], with no reference to the microscopic reversibility hypothesis, whose validity remains instead controversial [32].

4 Model Development

4.1 Conservation Law.

As mentioned in the previous section, we here consider the ECM as a three-phase medium composed of a solid polymer network with fixed charges, a solvent (i.e. water molecules, interstitial fluid) and solutes (freely moving charges).

As the tissue deforms, the material element originally located at $\mathbf{X}$ in the initial configuration $\mathcal{B}_0$ is displaced to the point $\mathbf{x}$ in the current configuration $\mathcal{B}_t$, see Figure 3. Such transformation is described by the deformation gradient tensor $\mathbb{F} = \partial\mathbf{x}/\partial\mathbf{X}$; the information about the change in ECM volume is encoded

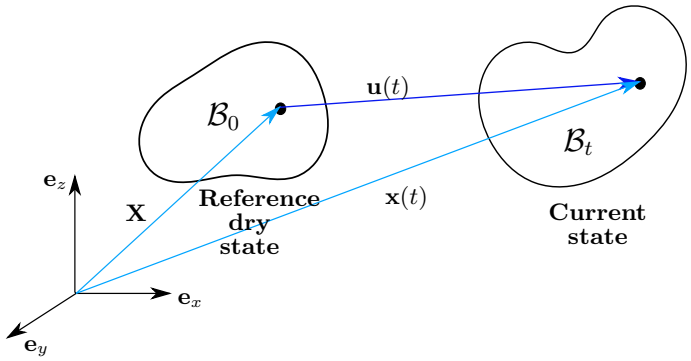

Fig. 3: Sketch of the dry and current state of the ECM network.

in $J = \det \mathbb{F}$. As in [24], we consider the reference, or initial, state $\mathcal{B}_0$, which is stress free, to be equivalent to the dry stage of the ECM, i.e. only solid phase present. Since we assume the solid phase to be incompressible, any change in the volume can only be related to the migration of solvent and solutes molecules, whose nominal concentrations will be denoted by C_s and C_i respectively, $i = 1, \ldots, N$ with N being the number of free ion species. This lead to the molecular incompressibility condition:

$$J = 1 + v_s C_s + \sum_{i=1}^{N} v_i C_i \tag{9}$$

where v_m are the characteristic molecular volume of each species in the solution. When considering the interstitial fluid, the contribution of ions to the volume can be neglected [47,48] so that Equation (9) reduces to:

$$J = 1 + v_s C_s. \tag{10}$$

Consequently, the volume fractions of fluid ϕ_f and solid ϕ_n phases in the gel are defined as:

$$\phi_f = \frac{v_s C_s}{1 + v_s C_s}, \qquad \phi_n = \frac{1}{1 + v_s C_s}. \tag{11}$$

where again we are neglecting the contribution of ions to the total volume. While C_m denote the number of each molecule per unit volume in the initial configuration for the m-th species in the solution, the actual concentration in the current state is denoted by $c_m = C_m/J$. Throughout the derivation of the model, we will be using the index $i = 1, \ldots, N$ to denote the ionic species only, while $m \in \{s, 1, \ldots, N\}$ refers to all mobile species, i.e. both the solvent and solutes.

Mass conservation must apply to all mobile species and in the initial configuration this reads:

$$\dot{C}_m + \nabla_0 \cdot \mathbf{J}_m = 0, \tag{12}$$

where $\mathbf{J}_m$ is the nominal flux per unit area in the dry state, $\dot{C}_m$ is the derivative of C_m with respect to time, i.e. $\dot{C}_m \equiv \partial_t C_m$ and ∇_0 denote the gradient in the

Lagrangian coordinates $\mathbf{X}$. Their counterparts in the actual configuration are denoted by $\mathbf{j}_m$ and ∇ and are defined according to the following rules:

$$\mathbf{J}_m = J\mathbb{F}^{-1}\mathbf{j}_m, \qquad \nabla_0(\cdot) = \mathbb{F}^T\nabla(\cdot). \tag{13}$$

When considering tissues or hydrogels, inertial and gravitational effect are commonly neglected, so that the conservation of momentum for the ECM reads:

$$\nabla_0 \cdot \mathbb{S} = 0, \tag{14}$$

where $\mathbb{S}$ is the first Piola-Kirchoff tensor, which represents the stress state of the ECM in the initial configuration. The counterpart in the current configuration is the Cauchy stress tensor $\mathbb{T}$, which is related to $\mathbb{S}$ as follows:

$$\mathbb{T} = J^{-1}\mathbb{S}\mathbb{F}^T. \tag{15}$$

The presence of free moving ions generates an electric field which is denoted by $\mathbf{E}$ and $\mathbf{e}$ in the initial and current configuration respectively. Introducing the electrostatic potential Φ, we have that:

$$\mathbf{E} = -\nabla_0 \Phi, \qquad \mathbf{e} = -\nabla \Phi. \tag{16}$$

As in [25], we consider the matrix to be a dielectric material[2]. Consequently, the presence of the electric field generates an electric displacement $\mathbf{H}$[3], which must obey Gauss law of electrostatics:

$$\nabla_0 \cdot \mathbf{H} = Q, \tag{17}$$

where Q is the local total charge, which accounts for both fixed and moving charges:

$$Q = e\left(\sum_i z_i C_i + z_f C_f\right), \tag{18}$$

where e is the elementary charge, C_f is the concentration of fix charges and z_m is the valence of the corresponding charged species. Note that C_f here corresponds to the concentration of GAGs, which is assumed to be a constant a fraction of C_s. As for above, we can move from nominal quantities to the corresponding value in the current configuration by applying the following rules:

$$\mathbf{H} = J\mathbf{h}\mathbb{F}^{-T}, \tag{19}$$

$$\mathbf{E} = \mathbb{F}^T\mathbf{e}, \tag{20}$$

where $\mathbf{h}$ is the electric displacement in the current configuration.

[2] an electrical insulator, which can be polarized in the presence of an electric field.

[3] the vector field that accounts for both the electric field and the polarization of the dielectric material.

4.2 Kinematics.

As mentioned in the introduction, we model the ECM as a poro-visco-elastic material, with particular interest in the viscous aspect of the material. As shown in Figure 4, there are two molecular processes that give rise to the macroscopic time-dependent response of the system:

1. the rearrangements of molecules at the micro-scale, which has entropic origin and result in a volume-preserving viscous deformation;
2. the long range transport of fluid that leads to swelling, i.e. changes in the ECM's size.

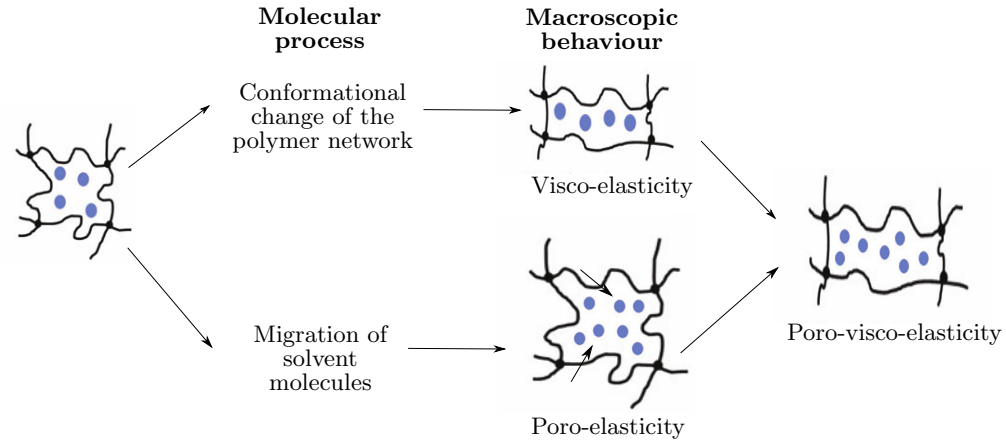

Fig. 4: Illustration of the molecular processes which account for the macroscopic deformation of ECM: viscosity is related to change in the conformation of the network which preserve the volume of the network.

As illustrated in Figure 4, at the microscopic level this results in a visco-elastic and poro-elastic behaviour respectively.

In order to capture both phenomena, as common in the large-deformation theory [10,11,1,22,39,46] and first proposed by Kröner in 1960 [30], we consider a multiplicative decomposition of the deformation tensor $\mathbb{F}$. As this can be choose arbitrary, different decomposition have been proposed in the literature. We will here consider the two most commonly used, which will be here denoting by model A [10,11,1] and model B [22,39,21]:

$$\text{MODEL A} \Rightarrow \begin{cases} \mathbb{F} = \mathbb{F}_e \mathbb{F}_v, \\ \det \mathbb{F}_v = 1, \quad \det \mathbb{F}_e = \det \mathbb{F} \end{cases} \tag{A}$$

$$\text{MODEL B} \Rightarrow \begin{cases} \mathbb{F} = \mathbb{F}_{vol} \bar{\mathbb{F}} = \mathbb{F}_{vol} \bar{\mathbb{F}}_e \bar{\mathbb{F}}_v \\ \det \mathbb{F} = \det \mathbb{F}_{vol}, \quad \det \bar{\mathbb{F}} = \det \bar{\mathbb{F}}_e = \det \bar{\mathbb{F}}_v = 1. \end{cases} \tag{B}$$

Comparing the two, we note that the only difference is that in model B the volumetric deformation, $\mathbb{F}_{vol}$, is decoupled from the deviatoric one, $\bar{\mathbb{F}}$. To the best of our knowledge, there is no previous systematic study in the literature that compares these two approaches. As it will be clear in Section **??**, the choice of how to decompose the vector $\mathbb{F}$ is not only a mathematical argument but also affect the constitutive assumption on the material properties. This highlights the need of experimental testing to validate which model better describe the material studied.

As an explanatory example of the derivation of a model in the non-equilibrium thermodynamics framework, we will fully derive in the main text only the governing equation for model A. The interested reader can find the details of the derivation for model B in Appendix D.

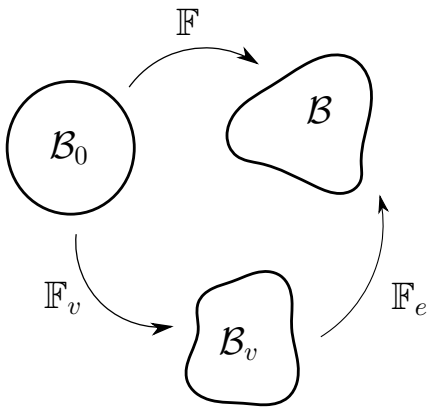

Fig. 5: multiplicative decomposition corresponding to model A, Equation (A).

Looking back at Equation (A), $\mathbb{F}_e$ is the elastic contribution to the deformation while, the term $\mathbb{F}_v$ accounts for the viscous flow. As illustrate in Figure 5, the multiplicative decomposition is equivalent to introducing an intermediate configuration $\mathcal{B}_v$, called the natural or virtual configuration. The evolution of the natural configuration can be interpreted as an entropy producing, i.e. dissipative, process. On the other hand, in the elastic deformation from the natural to the current configuration energy is only stored in the system.

Using Equation (A), we can compute the velocity gradient tensor $\mathbb{L}$:

$$\mathbb{L} = \dot{\mathbb{F}}\mathbb{F}^{-1} = \mathbb{L}_e + \mathbb{F}_e\mathbb{L}_v\mathbb{F}_e^{-1}, \tag{21}$$

where $\mathbb{L}_e = \dot{\mathbb{F}}_e\mathbb{F}_e^{-1}$ and $\dot{\mathbb{F}}_v\mathbb{F}_v^{-1}$ are respectively the elastic and viscous velocity gradient tensor. These can be decomposed in their symmetric $\mathbb{D}$ and skewed $\mathbb{W}$ part:

$$\begin{aligned} \mathbb{L}_e = \mathbb{D}_e + \mathbb{W}_e, \quad \mathbb{D}_e = \frac{\mathbb{L}_e + \mathbb{L}_e^T}{2}, \quad \mathbb{W}_e = \frac{\mathbb{L}_e - \mathbb{L}_e^T}{2}; \\ \mathbb{L}_v = \mathbb{D}_v + \mathbb{W}_v, \quad \mathbb{D}_v = \frac{\mathbb{L}_v + \mathbb{L}_v^T}{2}, \quad \mathbb{W}_v = \frac{\mathbb{L}_v - \mathbb{L}_v^T}{2}. \end{aligned} \tag{22}$$

The decomposition (A) is not unique, as stress state in $\mathcal{B}_v$ would not change under any arbitrary rigid-body rotation [35]. As suggested by [1], in the case of isotropic material, it is reasonable to assume the viscous flow to be irrotational, i.e. $\mathbb{W}_v = \mathbb{O}$, so that $\mathbb{L}_v \equiv \mathbb{D}_v$. As mentioned before, the physical nature of the viscous deformation is molecular rearrangement so that volume is preserved. This requires to introduce the additional constraint:

$$J_v = \det \mathbb{F}_v = 1. \tag{23}$$

4.3 Energy Balance Inequality.

As mentioned in Section 3, according to how the system exchanges energy and mass with the environment, the energy imbalance imposes restrictions on the free energy ψ. Considering a control volume R in the reference configuration $\mathcal{B}_0$, the system exchanges mass due to the diffusion of each mobile species, so that $M(R)$ is given by:

$$M(R) = \sum_{m=s,1,\dots,N} -\int_{\partial R} \mu_m \, \mathbf{J}_m \cdot \mathbf{n} \tag{24}$$

where $\mathbf{n}$ is the unit normal vector to the surface ∂R and μ_m is the chemical potential associated with each species. Widely used in the thermodynamics of mixture, the chemical potential is a measure of the rate of change in free energy associated with adding one more molecule to a unit volume.

The term $W(R)$, i.e. the rate of work done on the system, is instead decomposed in two contributions, the rate of electrical $W_{el}(R)$ and mechanical work $W_{mec}(R)$. Following [18], $W_{el}(R)$ is defined as:

$$W_{el}(R) = -\int_{\partial R} \Phi \, \dot{\mathbf{H}} \cdot \mathbf{n} \tag{25}$$

Following the work of Gurtin [23], we account both for the presence of macro-stresses $\mathbb{S}$ and micro-stresses $\boldsymbol{\xi}$, which arise due to the system heterogeneity [31]. As before we only consider the dominant contribution of the solvent while neglecting the solute, so that $W_{mec}(R)$ reads:

$$W_{mec}(R) = \int_{\partial R} (\boldsymbol{\xi} \cdot \mathbf{n}) \, \dot{C}_s + \int_{\partial R} \mathbb{S}\mathbf{n} \cdot \dot{\mathbf{u}} \tag{26}$$

where $\mathbf{u} = \mathbf{x} - \mathbf{X}$ is the displacement vector, which is related to the deformation tensor by $\mathbb{F} = \mathbb{I} - \nabla_0 \mathbf{u}$. Substituting this result back into the formula (2) and applying the divergence theorem we obtain the following inequality:

$$\int_R \dot{\psi} - \mathbf{E} \cdot \dot{\mathbf{H}} + \sum_{i=1}^{N} \left[e\Phi z_i \dot{C}_i + \nabla_0 \left(\mu_i \mathbf{J}_i \right) \right] + \nabla_0 (\mu_s \mathbf{J}_s - \boldsymbol{\xi} \dot{C}_s - \mathbb{S}^T \dot{\mathbf{u}}) \leq 0 \tag{27}$$

Since this must hold for any choice of the volume R, the inequality must hold also locally:

$$\dot{\psi} - \mathbf{E}\cdot\dot{\mathbf{H}} + \sum_{i=1}^{N}\left[e\Phi z_i\dot{C}_i + \nabla_0\left(\mu_i\mathbf{J}_i\right)\right] + \nabla_0(\mu_s\mathbf{J}_s - \boldsymbol{\xi}\dot{C}_s - \mathbb{S}^T\dot{\mathbf{u}}) \leq 0. \tag{28}$$

Further accounting for Equations (12)-(14), we obtain that:

$$\begin{aligned}\dot{\psi} - \mathbf{E}\cdot\dot{\mathbf{H}} + \sum_{i=1}^{N}\left[e\Phi z_i - \mu_i\right]\dot{C}_i - \left(\mu_s + \nabla_0\cdot\boldsymbol{\xi}\right)\dot{C}_s - \mathbb{S}:\dot{\mathbb{F}} \\ -\boldsymbol{\xi}\cdot\nabla_0\,\dot{C}_s + \sum_m \nabla_0\,\mu_m\cdot\mathbf{J}_m \leq 0.\end{aligned} \tag{29}$$

As exhaustively discussed in previous studies [1,23], the energy inequality imposes restrictions on the constitutive equation of the free energy ψ. Adapting their results to our specific problem, we have that:

$$\psi = \psi(\mathbb{F}, \mathbb{F}_e, C_s, C_i, \nabla_0\,C_s, \mathbf{H}), \tag{30}$$

which precludes any explicit dependency of ψ on the chemical potential or the viscous deformation gradient $\mathbb{F}_v$. By differentiating the incompressibility condition (10) and (23), we obtain:

$$v_s\dot{C}_s - J\mathbb{F}^{-T}:\dot{\mathbb{F}} = 0, \tag{31}$$

$$\mathbb{I}:\mathbb{L}_v = 0. \tag{32}$$

If we now substitute (30) into (29), and include the constraint (31)-(32) using as Lagrange multipliers p and p_v respectively, we are left with the augmented form of the energy imbalance inequality:

$$\begin{aligned}\left(\frac{\partial\psi}{\partial\nabla_0 C_s} - \boldsymbol{\xi}\right)\cdot\nabla_0\dot{C}_s + \left(\frac{\partial\psi}{\partial C_s} - \mu_s - \nabla_0\cdot\boldsymbol{\xi} + pv\right)\dot{C}_s \\ + \sum_i\left(\frac{\partial\psi}{\partial C_i} + e\Phi z_i - \mu_i\right)\dot{C}_i + \left(\frac{\partial\psi}{\partial\mathbf{H}} - \mathbf{E}\right)\cdot\dot{\mathbf{H}} \\ + \left(\frac{\partial\psi}{\partial\mathbb{F}} + \frac{\partial\psi}{\partial\mathbb{F}_e}\mathbb{F}_v^{-1} - \mathbb{S} - pJ\mathbb{F}^{-T}\right):\dot{\mathbb{F}} + \sum_m \nabla_0\,\mu_m\cdot\mathbf{J}_m \\ -\left(\mathbb{F}_e^T\frac{\partial\psi}{\partial\mathbb{F}_e} - p_v\mathbb{I}\right):\mathbb{L}_v \leq 0.\end{aligned} \tag{33}$$

Note that in deriving (33), we have also made us of the following identity:

$$\dot{\mathbb{F}} = \dot{\mathbb{F}}_e\mathbb{F}_v + \mathbb{F}_e\dot{\mathbb{F}}_v \Longrightarrow \dot{\mathbb{F}}_e = \dot{\mathbb{F}}\mathbb{F}_v^{-1} - \mathbb{F}_e\mathbb{L}_v. \tag{34}$$

4.4 Construction of the Free Energy.

Having the general form of ψ, Equation (30), it remains to construct its precise form. Following a standard approach in ψ-depending modeling, we assume that the total free energy can be additively decomposed with each physical mechanisms contributing independently. We here consider six distinct contributions:

- the energy of the electric field ψ_1;
- the energy of solvent and solutes' molecules not interacting with the solid phase ψ_2;
- the energy of mixing the solid phase with the solution, ψ_3;
- the energy of mixing the solvent with the solutes in solution, ψ_4;
- the interfacial energy between dissimilar phases, ψ_5;
- the energy of the solid phase not interacting with the solution, ψ_6.

Assuming the solid phase to be an ideal and linear dielectric material, with constant permittivity ϵ,the free energy of polarization reads [17,25]:

$$\psi_1 = \frac{1}{2\epsilon J}\mathbf{H}\mathbb{F}^T \cdot \mathbb{F}\mathbf{H}. \tag{35}$$

The specific energy density ψ_2 has the standard form:

$$\psi_1 = \sum_m \mu_m^0 C_m \tag{36}$$

where μ_m^0 denotes the chemical potential of non interacting solvent and ions molecules. According to Flory-Huggins theory [19,28] of mixtures, the mixing energy is given by:

$$\psi_3 = \frac{k_B T J}{v_s}\left(\phi_f \ln \phi_f + \chi \phi_f \phi_n\right), \tag{37}$$

where k_B is the Boltzmann's constant, T is the temperature and χ is the Flory-Huggins parameter, which is a measure of the enthalpy of mixing. Different is the approach of Xue et al. in [47,48]. In these studies, the authors assume only the mixing of GAGs with solvent, while neglecting the collagen. Since we are considering GAGs and the collagen network as as a unique solid phase and we could not find any evidence that collagen does not mix with water, we have chosen the more general form (37).

As the interstitial fluid is well approximated by a dilute solution, the contribution ψ_4 reads [25,47,48]:

$$\psi_4 = k_B T \sum_{i=1}^{N} C_i \left(\ln \frac{C_i}{C_s} - 1\right). \tag{38}$$

As proposed by Hong et al. [26], we include in the energy the effect of interface tension. Despite having been neglected in many models for hydrogel swelling, this term plays a role in the transient poroelastic relaxation of the material, when boundaries between solvent-rich and solvent-poor regions can emerge [24,26].

Again we assume that the contribution of mobile ions is negligible, so that only the solid-solvent interface contributes to the energy:

$$\psi_5 = \frac{\gamma}{2} J \left|\nabla C_s\right|^2, \tag{39}$$

where the constant γ plays a role analogous to a surface tension.

Finally, we need to specify the strain energy ψ_6 which depends on the particular constitutive model used to describe the material. As mentioned in the Introduction the Standard Linear Solid (SLS), see Figure 1, is commonly used to describe soft material in the regime of small deformation. However, when account for large deformation, as in the case of swelling, soft material present a non-linear behaviour. For this reason we consider the model in Figure 6a, which is a generalization of the 1D SLS to 3D problems with non-linear elastic response.

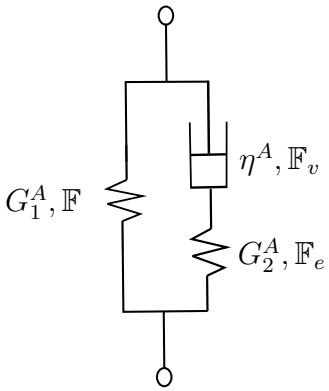

(a)

Element	Constitutive Properties	Deformation
spring 1	Isotropic Neo-Hookean spring	volumetric + deviatoric
spring 2	Isotropic Neo-Hookean spring	volumetric + deviatoric
dashpot	Isotropic Linear dashpot	deviatoric

(b)

Fig. 6: (a) Schematic representation of the non-linear rheological model for ECM; (b) Table summarizing the major properties of the model components.

The strain energy can thus be decomposed into the sum of the contributions from spring 1 and spring 2:

$$\psi_6 = \psi_1(\mathbb{F}) + \psi_2(\mathbb{F}_e). \tag{40}$$

As in [48], we consider the spring to be isotropic and hyper-elastic (Neo-Hookean) which are characterised by the following form of the free-energy:

$$\psi_1(\mathbb{F}) = \frac{G_1^A}{2} \left(\mathbb{F} : \mathbb{F} - 3 - 2\ln J\right) \tag{41}$$

$$\psi_2(\mathbb{F}_e) = \frac{G_2^A}{2} \left(\mathbb{F}_e : \mathbb{F}_e - 3 - 2\ln J_e\right) \tag{42}$$

where $G_\cdot$ stands for the shear modulus associated with each spring, $J_e = \det \mathbb{F}_e$, while J is as defined in the previous sections. As derived in [20], the hyper-elastic model (42) can be correlated to the microscopic properties of a polymer network, under the assumption of Gaussian chains and affine deformation. Other

thermodynamically consistent form of the stretching energy have been proposed in the literature [4,7,15]. These have been also derived by statistical arguments but starting from different network models.

4.5 Entropy Production σ.

Having specified how the system interacts with its environment, we can now discuss how it dissipates energy. As mentioned in Section (4.2), there are two contributions: transport (diffusion of solvent and solutes) and viscosity. The thermodynamic fluxes [4] associated with these two phenomena are $\mathbf{J}_m$, $m = s, 1, \ldots, N$, and $\mathbb{L}_v$. Consequently, using Equation (5), we obtain:

$$\sigma = \sum_m \zeta_m \cdot \mathbf{J}_m + \zeta_v : \mathbb{L}_v, \tag{43}$$

where ζs represent the thermodynamic forces associate with each flux. On the other hand, $\nabla_0 \dot{C}_s$, $\dot{C}_s$, $\dot{C}_i$, $\dot{\mathbf{H}}$ and $\dot{\mathbb{F}}$ describe the evolution of reversible process. This implies that their value can be controlled and arbitrarily chosen, by carefully tune the condition of an experiment, while the energy imbalance inequality (33) continue to hold. Given the constraint (30) on ψ, this can only happen if the terms highlighted in blue in Equation (33) are identically zero. As shown in the Appendix [TO DO], this leads to the following system of equations:

$$\boldsymbol{\xi} = \gamma J\, \mathbb{B}^{-1}\, \nabla_0\, C_s, \tag{44}$$

$$\begin{aligned} \mu_s = p v_s + \mu_s^0 - \gamma J \nabla^2 C_s + k_B T \Bigg[\ln \frac{C_s v_s}{1 + C_s v_s} + \frac{1}{1 + C_s v_s} \\ + \frac{\chi}{(1 + C_s v_s)^2} - \sum_i \frac{C_i}{C_s} \Bigg], \end{aligned} \tag{45}$$

$$\mu_i = \mu_i^0 + e\Phi z_i + kT \ln \frac{C_i}{C_s}, \tag{46}$$

$$\mathbf{E} = \frac{1}{\epsilon J} \mathbb{F}^T \mathbb{F}\, \mathbf{H}\,, \qquad -\epsilon J \nabla^2 \Phi = Q\,, \tag{47}$$

$$\begin{aligned} \mathbb{T} = -p\mathbb{I} + \underbrace{\gamma \left[\frac{1}{2} |\nabla C_s|^2 \mathbb{I} - \nabla C_s \otimes \nabla C_s \right]}_{\mathbb{T}^{kort}} + \underbrace{\epsilon \left[\frac{1}{2} |\nabla \Phi|^2 \mathbb{I} - \nabla \Phi \otimes \nabla \Phi \right]}_{\mathbb{T}^{Max}} \\ + \frac{G_1^A}{1 + C_s v_s} (\mathbb{B} - \mathbb{I}) + \frac{G_2^A}{1 + C_s v_s} (\mathbb{B}_e - \mathbb{I})\,, \end{aligned} \tag{48}$$

As discussed in Section 3, in the framework of linear non-equilibrium thermodynamics, when considering isothermal transformation, the second law of thermodynamics can be rewrite as Equations (8). Using the same argument as

[4] See Section 3

in Section 4.3 and Equation (43), we can rewrite Equations (8) in differential form, and substituting Equations (44)-(48), we obtain:

$$\sigma = -\sum_m \frac{1}{T}\nabla_0 \mu_m \cdot \mathbf{J}_m + \frac{1}{T}\left(\mathbb{F}_e^T \frac{\partial \psi}{\partial \mathbb{F}_e} - p_v \mathbb{I}\right) : \mathbb{L}_v \tag{49}$$

Equating Equation (49) and (43), it is evident that the thermodynamics forces are:

$$\zeta_m = \frac{1}{T}\nabla_0 \mu_m, \tag{50}$$

$$\zeta_v = \frac{1}{T}\left(\mathbb{F}_e^T \frac{\partial \psi}{\partial \mathbb{F}_e} - p_v \mathbb{I}\right) = \frac{1}{T}\left[G_2^A(\mathbb{C}_e - \mathbb{I}) - p_v \mathbb{I}\right]. \tag{51}$$

Assuming to be in regime of linear non-equilibrium thermodynamics, we can use the identity (6) to couple fluxes and forces. However, considering the symmetry constraint from *Curie's law*[5] , there can be no coupling between fluxes and forces of different tensorial nature. Consequently, we are left with the following force-flux relation:

$$\mathbb{L}_v = L_{vv}\zeta_v, \tag{52}$$

$$\mathbf{J}_m = \sum_{k=s,1,\dots,N} L_{mk}\zeta_k. \tag{53}$$

As described in Appendix C, starting from Equations (50)-(53) and with common consideration from the theory of mixture, we can derive the following system of time dependent equations:

$$\partial_t C_s = \nabla_0 \cdot \left[K C_s \mathbb{F}^{-1}\left(c_s \nabla \mu_s + \sum_i \frac{D_i}{D_i^0} c_i \nabla \mu_i\right)\right], \tag{54}$$

$$\partial_t C_m = \nabla_0 \cdot \left[\frac{D_i}{k_B T} C_i \mathbb{F}^{-1} \nabla \mu_i - \frac{D_i}{D_i^0}\frac{C_i}{C_s} J \mathbb{F}^{-1} \mathbf{J}_0\right], \tag{55}$$

$$\dot{\mathbb{B}}_e = \mathbb{L}\mathbb{B}_e + \mathbb{B}_e \mathbb{L}^T - \frac{1}{\tau_R}\mathbb{B}_e \mathrm{DEV}[\mathbb{B}_e]. \tag{56}$$

where the parameters are macroscopic phenomenological coefficients, that can either be estimated experimentally or derived from the nano/microscopic properties of the different phases [47,48]. To sum up the governing equations for the Model A are Equations (45)-(48) together with the flow rules (54)-(56). The analogous system of equation for model B can be found in Appendix D.

[5] Macroscopic causes can not have more element of symmetries than the effect they cause [32]

4.6 Transport Equation.

In order to get a better physical insight into the behaviour, we first rewrite the solvent chemical potential as:

$$\mu_s = \mu_s^0 + k_B T \left(\frac{p v_s}{k_B T} + \Pi_{osm} - \sum_i \frac{C_i}{C_s} - \frac{\gamma J}{k_B T} \Pi_{grad} \right), \tag{57}$$

$$\Pi_{osm} = \ln \frac{C_s v_s}{1 + C_s v_s} + \frac{1}{1 + C_s v_s} + \frac{\chi}{(1 + C_s v_s)^2}, \tag{58}$$

$$\Pi_{grad} = \nabla^2 C_s, \tag{59}$$

where p represents the pore pressure, Π_{osm} is the osmotic pressure of the solution and Π_{grad} is the pressure due to interface energy. If we now substitute into Equations (54) the chemical potentials (57)-(46), which yields to:

$$\begin{aligned} \partial_t C_s = \nabla_0 \cdot \Bigg\{ K \mathbb{F}^{-1} \Bigg[C_s v_s \nabla p - \gamma C_s J \nabla \Pi_{grad} + \sum_i \frac{D_i}{D_i^0} C_i e z_i \nabla \Phi \\ + k_B T \left(C_s \nabla \Pi_{osm} + \sum_i \left(1 - \frac{D_i C_i}{D_i^0 C_s} \right) \nabla C_s - \sum_i \left(1 - \frac{D_i}{D_i^0} \right) \nabla C_i \right) \Bigg] \Bigg\}. \end{aligned} \tag{60}$$

The above equation shows that the solvent transport is driven by pressure gradient, osmotic pressure gradient, electric potential gradient and the additional interface term, which has not been considered in the context of polyelectrolytes. In the absence of solutes ($C_i \equiv 0$), we recover the same model presented by Hennessy et. al [24]. If we further assume that $|\nabla \Pi_{grad}| << 1$ and take the limit $v_s C_S \to \infty$, Equations (60) reduces to Darcy's law for the flow in a porous media. The model for polyelectrolytes proposed by Hong [25] correspond instead to the limit $D_i^0 \to \infty$, i.e. mobile species can move freely in pure solution, and $|\nabla \Pi_{grad}| << 1$.

Similarly we can rewrite Equation (55) as:

Having concluded the derivation of the model, we are now interested in comparing the two model in different experimental settings: free swelling and compression test. For the second case, after using a numerical study *in silico*, we will also test the two models on real data collected by Netti et al. [38] from compression test on tumour extracellular matrix.

In all simulation, unless differently stated, we will use the parameters in Table 1 will be considered to be constant [38,48].

5 Unconstrained Free Swelling.

We here consider the first experimental setup: unconstrained free swelling. In such situation, we consider the ECM is left free to swell in bath of interstitial solution. As the system evolves, the ECM increases in size until it reaches a steady state. As in [18], we are assume that at equilibrium:

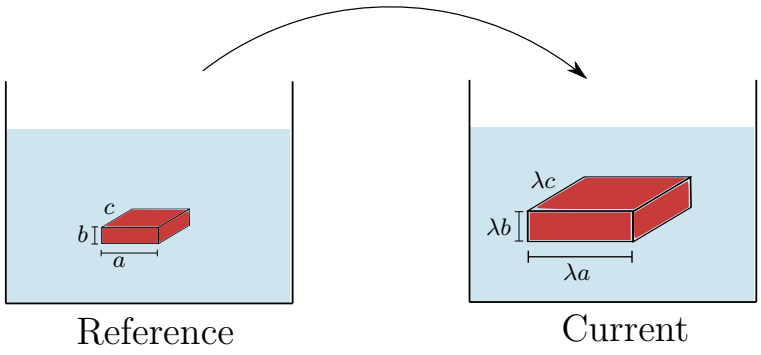

Fig. 7: Schematic representation of a free swelling. Since we are considering an isotropic mixture, the ECM maintains its shape while all dimension are stretched of the same amount λ. So that the relative volume change is $\delta V = \lambda^3 - 1$.

1. chemical potentials of solvent and solutes is homogeneous and equal in the bath and in the bath:

$$\mu_s = \mu_s^{ext} = \mu_s^0 - vkT \sum_i c_0^i, \tag{61}$$

$$\mu_i = \mu_i^{ext} = \mu_i^0 + kT \ln(v_s c_0^i), \tag{62}$$

   where the bath solution is assumed to be neutral with a potential $\phi^{bath} = 0$.
2. The electrostatic potential and the solute concentration are constant in the ECM, but different to the value in the bath. This difference creates a thin charged interface at the boundary, whose thickness is negligible compared to the size of the ECM.
3. The contribution of $\mathbb{T}^{Max}$ and $\mathbb{T}^{kort}$to the stress at this interface can be neglected compared to the mechanical stress due to the deformation.
4. The bath is in a stress free configuration so as the ECM at equilibrium:

$$\mathbb{T} = 0. \tag{63}$$

Finally, to investigate the equilibrium, we specify the deformation gradient tensor, which is of the form:

$$\mathbb{F} = \lambda \mathbb{I}, \tag{64}$$

with $\lambda = (1 + C_s v_s)^{1/3}$. To simplify, we also assume that there are only two species of ions in the solution: a positive C_+ with $z_+ = 1$ and a negative one C_- with $z_- = -1$. Since the bath solution is neutral, the total charge must vanish, $c_0^+ = c_0^- = c_0$.

Throughout the work, unless differently specified, we will use the parameters in Table 1 will be considered to be constant so to reflect the condition in the experiment by Netti et al. [38,48].

5.1 Model A.

In the case of free swelling, due to the symmetry of $\mathbb{F}$, it reasonable to assume that also $\mathbb{F}_e$ is of the similar form, $\mathbb{F}_e = \lambda_e \mathbb{I}$. Consequently, based on Equation (94) in

Symbol	Value	Unit
C_f	3.947×10^{23}	m^{-3}
v_s	3×10^{-29}	m^3
z_f	-4	-
k_B	1.38×10^{-23}	J/K
T	295	K
c_0^i	9.27×10^{25}	m^{-3}

Table 1: Parameters adopted in the simulations as estimated in [48] in reference to the experiment by Netti et al. [38].

Appendix C, we have that the viscous contribution vanish so that $\mathbb{B}_e = \mathbb{B} = \lambda^2 \mathbb{I}$. Substituting this result and the boundary condition (62)-(63) into Equations (44)-(47) and (48), setting to zero all spatial derivative, we obtain:

$$p_A = \frac{G_1^A + G_2^A}{1 + C_s v_s}(\lambda^2 - 1), \tag{65}$$

$$\Pi_A^n = \frac{k_B T}{v_s}\left[\ln \frac{C_s v_s}{1 + C_s v_s} + \frac{1}{1 + C_s v_s} + \frac{\chi}{(1 + C_s v_s)^2}\right], \tag{66}$$

$$\Pi_A^{ion} = k_B T \sum_i \left(\frac{C_i}{v_s C_s} - c^0\right), \tag{67}$$

$$0 = \frac{v_s}{k_B T}(p_A + \Pi_A^n - \Pi_A^{ion}), \tag{68}$$

$$0 = \pm \frac{e}{k_B T}\phi + \ln \frac{C_\pm}{C_s v_s c_\pm^0}, \qquad i = 1, \ldots, N, \tag{69}$$

$$Q = e\,(C_+ - C_- + z_f C_f) = 0. \tag{70}$$

where Π^n and Π_A^{ion} are the osmotic pressures due to the mixing of the polymer network with the solvent and the imbalance of ions inside and outside the ECM. Note that at equilibrium the system reaches a balance between the mechanical pressure p_A and the osmotic pressures. Moreover, the electro-neutrality condition is naturally imposed, Equation (70). As shown in Appendix , manipulating the above system we can reduce the number of unknown to the solvent concentration C_s:

$$C_\pm = \frac{1}{2}\left[\mp z_f C_f + \sqrt{(z_f C_f)^2 + (2 v_s C_s c_0)^2}\right], \tag{71}$$

$$\begin{aligned} F_A(C_s; c_0, \chi, G_{eq}^A) =& \frac{1 + C_s v_s + \chi}{(1 + C_s v_s)^2} + \frac{G_{eq}^A v_s}{k_B T}\frac{(1 + v_s C_s)^{2/3} - 1}{1 + C_s v_s} \\ &+ \ln \frac{C_s v_s}{1 + C_s v_s} + 2 c_0 v_s - \sqrt{\left(\frac{z_f C_f}{C_s}\right)^2 + 4 v_s^2 c_0^2} = 0 \end{aligned} \tag{72}$$

where $G^A_{eq} = G^A_1 + G^A_2$. Note that Equation (71) corresponds to the well known Donnan Equilibrium [18]. Equation (72) instead implicitly defines the concentration C_s and thus the final swelling volume. As expected, the latter can be controlled by changing the concentration of ions in the bath. We also notice that, free swelling experiment, are not sufficient to differentiate the elastic properties of the two branches as the two behave equivalently.

5.2 Models B.

In this second case, given the symmetry of the problem, we have that, at equilibrium the deviatoric component of the stress tensor $\mathbb{T}$ vanishes. Combining this information with the boundary condition and solving the system (115)-(119) for its equilibrium, we obtain the same equations as for model A, while the pressure is now defined as:

$$p = \frac{\partial \psi_{vol}}{\partial J}. \tag{73}$$

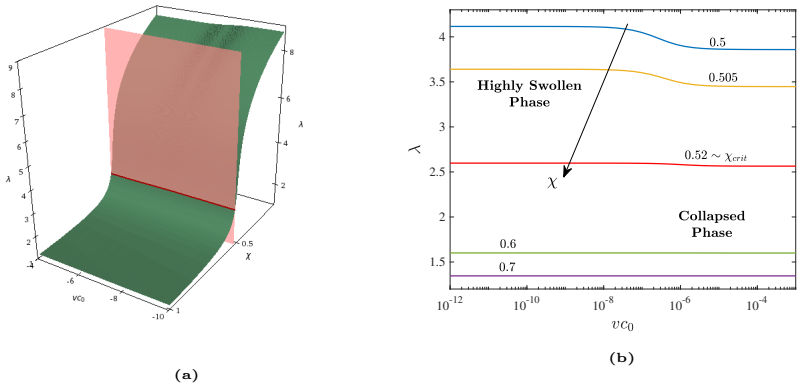

(a) (b)

Fig. 8: Free Swelling: (a) Manifold implicitly defined by Equation (72) where $G^A_{eq} = 10^3$ is fixed, while c_0 and χ are varied. On the vertical axis, we have plot λ as defined by (64). In the red, it is highlighted the plane corresponding to $\chi = \chi_{crit}$ that split the parameter space into the region of high swelling and collapse for the material [].

We follow two different approaches, in case BA, we derive the constitutive equation for ψ_{vol}, so that the model B and model A predict the same equilibrium behaviour, i.e. $p_A = p_{BA}$. Using Equations (65)-(73), and the constraint $\psi_{vol}(1) = 0$, we obtain:

$$\frac{\partial \psi^B_{vol}}{\partial J} = G^A_{eq}\frac{J^{2/3}-1}{J} \Longrightarrow \psi^B_{vol} = \frac{G_{vol}}{2}\left[3(J^{2/3}-1) - 2\ln J\right], \tag{74}$$

which is equivalent to using a Neo-Hookean model also for the volumetric spring with shear modulus G_{vol}. In the second case, we instead consider a more commonly used constitutive model for volumetric deformation.

6 Confined Compression Test.

In this second example, we consider to perform compression test on a previously swollen slice of ECM. As illustrated in Figure 9, a porous platen is used so that the fluids is free to flow and the chemical equilibrium with the external bath is restored after the transient relaxation phase. After compression of the tissue in ramps, the system is allowed to relax while the strain ϵ is maintained constant [38]. In this way, both the dynamical and equilibrium behaviour of the material can be assessed.

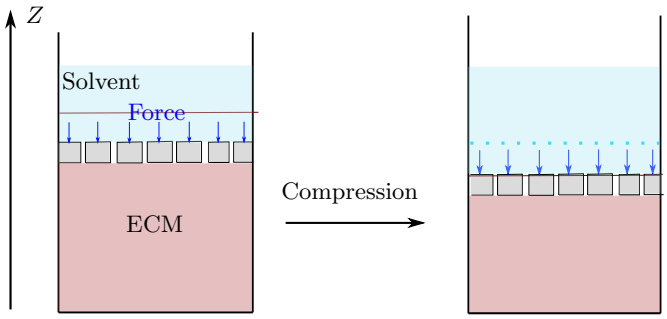

Fig. 9: Schematic representation of a compression test with a porous piston. A deformation is imposed in the Z direction and the force necessary to maintain the deformation is recorded.

As the deformation is constrained in Z direction, the deformation tensor is of the form:

$$\mathbb{F} = J_0^{1/3} \begin{bmatrix} 1 & 0 & 0 \\ 0 & 1 & 0 \\ 0 & 0 & \lambda_1 \end{bmatrix}, \tag{75}$$

where $\lambda_1 = 1 - \epsilon$. We here restrict our analysis to the equilibrium behaviour, for which the boundary conditions listed in Section 5 still hold with exception to the last one. Due to the external force $\mathbf{F} = -F_z \mathbf{e}_z$ which is exerted on the platen of area A, we now have that:

$$\mathbb{T} = \begin{bmatrix} 0 & 0 & 0 \\ 0 & 0 & 0 \\ 0 & 0 & \sigma \end{bmatrix}, \qquad \sigma = -\frac{F_z}{A}. \tag{76}$$

where $\mathbf{e}_z$ is the unit vector in the z direction in the current configuration. As we will see also in this simplified setting where the dynamics is neglected important differences emerges between the two model presented, which result in relevant quantitative predictions. Our aim is thus to understand under which information is necessary in order to discern which one better describe the material studied.

6.1 Model A

As before, given the symmetries of the system, $\mathbb{B}_e$ is a diagonal matrix of the form:

$$\mathbb{B}_e = \begin{bmatrix} b & 0 & 0 \\ 0 & b & 0 \\ 0 & 0 & b_1 \end{bmatrix}. \tag{77}$$

Again we are here interested in the equilibrium behaviour, for which Equations (71) still holds. Focusing on the contribution of spring B, studying the equilibriums of Equation (56), we obtain that $b = b_1$. Since $\det \mathbb{B}_e = (\det \mathbb{F})^2$, we conclude that:

$$b = J_0^{2/3}\lambda_1^{2/3}. \tag{78}$$

Using the boundary condition, we can now compute the pressure and the equilibrium condition:

$$p = -\sigma + \frac{G_1^A}{J_0\lambda_1}(J_0^{2/3}\lambda_1^2 - 1) + \frac{G_2^A}{J_0\lambda_1}(J_0^{2/3}\lambda_1^{2/3} - 1) \tag{79}$$

$$\begin{aligned} \frac{\sigma v_s}{k_B T} =& \frac{J_0\lambda_1 + \chi}{J_0^2\lambda_1^2} + \frac{G_1^A v_s}{k_B T}\frac{J_0^{2/3}\lambda_1^2 - 1}{J_0\lambda_1} + \frac{G_2^A v_s}{k_B T}\frac{J_0^{2/3}\lambda_1^{2/3} - 1}{J_0\lambda_1} \\ &+ \ln\frac{J_0\lambda_1 - 1}{J_0\lambda_1} + 2c_0 v_s - \sqrt{\left(\frac{z_f C_f v_s}{J_0\lambda_1 - 1}\right)^2 + 4v_s^2 c_0^2} \end{aligned} \tag{80}$$

6.2 Models B.

Based on Equation (75), we have that the tensors $\bar{\mathbb{B}}$ and $\bar{\mathbb{B}}_e$ are of the form:

$$\bar{\mathbb{B}} = \begin{bmatrix} \lambda_1^{-2/3} & 0 & 0 \\ 0 & \lambda_1^{-2/3} & 0 \\ 0 & 0 & \lambda_1^{4/3} \end{bmatrix}, \qquad \bar{\mathbb{B}}_e = \begin{bmatrix} \bar{b} & 0 & 0 \\ 0 & \bar{b} & 0 \\ 0 & 0 & \bar{b}_1 \end{bmatrix} \tag{81}$$

As for the model A, at equilibrium we have that $\bar{b} = \bar{b}_1$. However, in this case, we have that $\det \bar{B}_e = 1$ so that $\bar{b} = 1$ so that the second spring does not contribute to the stress. Using the boundary condition, in the case of model BA we obtain:

$$p_B = -\sigma + \frac{G_{vol}}{J_0\lambda_1}(J_0^{2/3}\lambda_1^{2/3} - 1) + \frac{2G_1^B}{3J_0\lambda_1^{5/3}}(\lambda_1^2 - 1) \tag{82}$$

$$\begin{aligned} \frac{\sigma v_s}{k_B T} =& \frac{J_0\lambda_1 + \chi}{J_0^2\lambda_1^2} + \frac{2G_1^B v_s}{3k_B T}\frac{\lambda_1^2 - 1}{J_0\lambda_1^{5/3}} + \frac{G_{vol} v_s}{k_B T}\frac{J_0^{2/3}\lambda_1^{2/3} - 1}{J_0\lambda_1} \\ &+ \ln\frac{J_0\lambda_1 - 1}{J_0\lambda_1} + 2c_0 v_s - \sqrt{\left(\frac{z_f C_f v_s}{J_0\lambda_1 - 1}\right)^2 + 4v_s^2 c_0^2}. \end{aligned} \tag{83}$$

Unlike the case of unconstrained swelling, we now have that the model A and BA are substantially different, so that there is no choice of the parameter that would predict the same stress-strain behaviour. This highlights how, the choice of a particular decomposition of the deformation gradient $\mathbb{F}$ correspond to a modelling decision on the constitutive properties of the material under study.

6.3 Model Comparison.

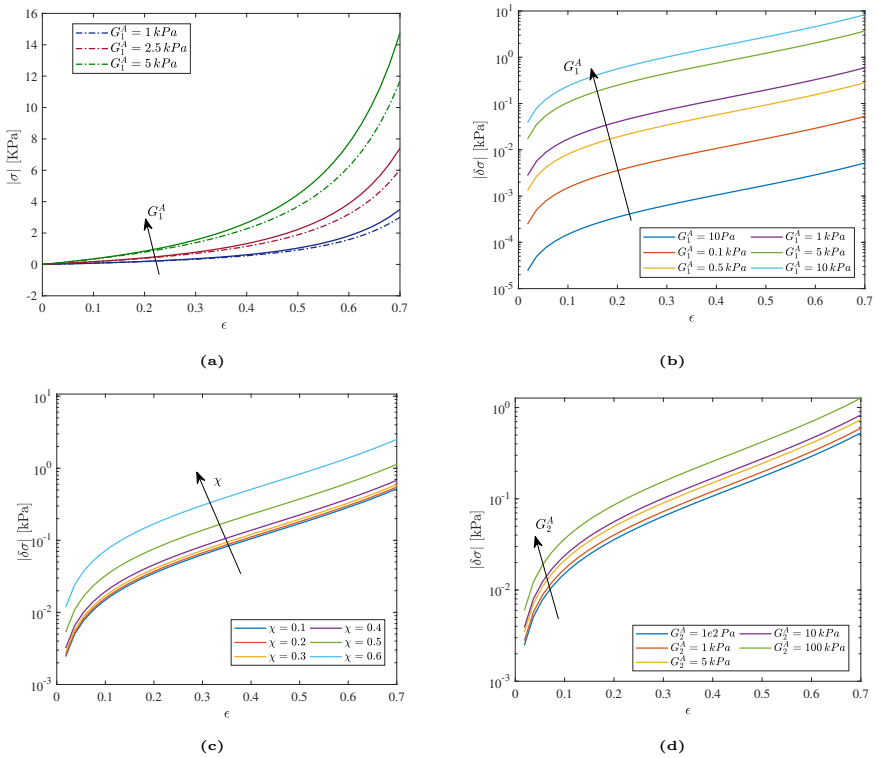

Fig. 10: Sensitivity Analysis. As expected the mismatch between the two model grows with the strain: (a) Comparison of stress-strain curve predicted by model A (dotted line) and model B (full line) for different value of the parameter G_1^A; (b) as G_1^A increase also the discrepancy $\delta\sigma$ grows; (c) $\delta\sigma$ is also particularly sensitive to changes in the mixing parameter χ, in particular we see that there is a relevant jump when the ECM is the *collapsed* phase; (d) on the other hand, only large changes in G_2^A have a relevant impact on $\delta\sigma$.

We first focus on comparing the model A and AB, assuming that the parameter χ is fixed and that $G_{vol} = G_{eq}^A$, so that the equilibrium volume J_0 is the same for both models. If we now take the difference between Equations (80) and (83), we obtain that the difference in the compression stress $\delta\sigma = \sigma_{BA} - \sigma_A$ is:

$$\delta\sigma = \frac{2G_1^B}{3}\frac{\lambda_1^2 - 1}{J_0\lambda_1^{5/3}} - \frac{G_1^A}{J_0^{1/3}}(\lambda_1 - \lambda_1^{-1/3}). \tag{84}$$

Looking at the above equation it appears clearly that there is no constant value of G_1^{AB} for which the difference $\delta\sigma$ is identically zero. If we impose that for small

deformation, i.e. $\lambda_1 \to 1$, the two models agree at the second order:

$$\delta\sigma = 0, \qquad \frac{\mathrm{d}\delta\sigma}{\mathrm{d}\lambda_1} = 0 \quad \Rightarrow \quad G_1^B = J_0^{2/3} G_1^A. \tag{85}$$

Under such condition we can rewrite the Equation (84) as:

$$\delta\sigma(\lambda_1; G_1^A, J_0) = \frac{G_1^A}{J_0^{1/3}\lambda_1^{5/3}} \left(\frac{2}{3}\lambda_1^2 - \frac{2}{3} - \lambda_1^{5/3} + \lambda_1^{4/3} \right), \tag{86}$$

which is unbounded for large deformation, i.e. $\lambda_1 \Rightarrow 0$. Note that J_0 is implicitly defined by Equation (72), where $J_0 = 1 + v_s C_s$. Consequently $\delta\sigma$ depends also on all the other parameters of the problem. As shown in Figure 10, χ plays an important role in determining the agreement between the two models. In our analysis, we have deliberately decided to look at absolute instead of relative differences. This is because when study the mechanical properties of materials, the order of magnitude are relevant in particular for scaffolds where pressure regulates the response of cells.

6.4 Test on Experimental Data.

In the previous section we have compared the two models assuming that data on free swelling are also available, so that G_{eq}^A, or equivalently G_{vol}, can be estimated separately, with all the other parameter known. However, this is not usually the case. In particular, when testing real tissues already swollen J_0 is not known and needs also to be estimated. Moreover, at our knowledge there are no studies on the estimation of the mixing parameter χ, so that this must be added to the list of unknown parameters.

Using the data collected by Netti et al. [38], we test the

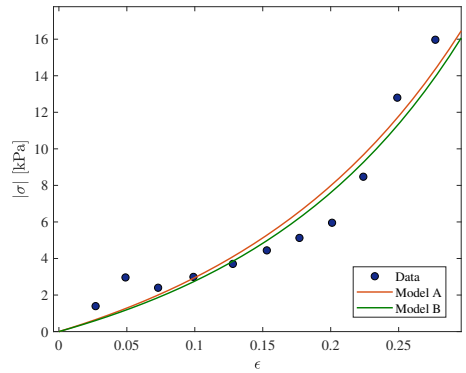

(a) Fitted Model

Model A		Model B	
χ	0.498	χ	0.524
G_1^A	18.9 kPa	G_{vol}	75 Pa
G_2^A	5.3 Pa	G_1^{BA}	55.1 kPa
J_0	20.7	J_0	14.8

(b) Estimated Parameters

Fig. 11: Comparison of the two model in fitting real experimental data from [38].

As shown in Figure 11a, both models are able to capture the qualitative behaviour of the data. However, as shown by the parameters in Table 11b, there are quantitative differences. In particular, there are order of magnitude of difference

in the estimated pressure p. If we look at its value for zero-strain, i.e. $\lambda_1 = 1$, we obtain:

$$p_A = \frac{G_1^A + G_2^A}{J_0}(J_0^{2/3} - 1) = \frac{24.2 \text{ kPa}}{20.7}(20.7^{2/3} - 1) = 7.64 \text{ kPa}, \tag{87}$$

$$p_{BA} = \frac{G_{vol}}{J_0}(J_0^{2/3} - 1) = \frac{0.075 \text{ kPa}}{14.8}(14.8^{2/3} - 1) = 25.5 \text{ Pa} \tag{88}$$

When designing synthetic ECM, the tuning of the internal pressure cells in a culture are exposed to is of large importance. As mentioned in the introduction, cells are sensitive to pressure and their response can greatly change depending on this stimulus. Consequently, depending on the model chosen, the

A Glossary of Variables and Parameters in the Model.

ψ	Helmholtz free energy per unit volume in the initial configuration,
$\mathbf{u}$	Displacement vector,
$\mathbb{F}$	Deformation gradient tensor $\mathbb{F} = \mathbb{I} - \nabla_0 \mathbf{u}$,
C_f	Concentration of fix charges in the network,
z_f	Charge of a GAG chain,
v_m	Characteristic molecular volume of the species m,
$\mathbf{u}$	Displacement vector,
$\mathbb{F}$	Deformation gradient tensor $\mathbb{F} = \mathbb{I} - \nabla_0 \mathbf{u}$,
$\mathbb{C}$	Right Cauchy-Green Tensor $\mathbb{C} = \mathbb{F}^T\mathbb{F}$,
$\mathbb{B}$	Left Cauchy-Green Tensor $\mathbb{B} = \mathbb{F}\mathbb{F}^T$,
$\mathbb{L}$	Velocity Gradient Tensor $\mathbb{L} = \dot{\mathbb{F}}\mathbb{F}^{-1}$,
J	Determinant of the deformation gradient tensor $J = \det \mathbb{F}$,
η^A	Viscosity of the collagen network in model A,
G_1^A	Shear modulus related to spring 1 in model A
G_2^A	Shear modulus related to spring 2 in model A
G_1^B	Shear modulus related to spring 1 in model B
G_2^B	Shear modulus related to spring 2 in model B
η^B	Viscosity of the collagen network in model A,
τ_R	Viscous relaxation time of the collagen network,
D_i^0	Diffusion coefficient for the i-th solute species when in pure solvent (interstitial fluid),
D_i	Diffusion coefficient for the i-th solute species in ECM,
K	Hydraulic permeability of the ECM to the interstitial fluid (solvent+solute),
k	Hydraulic permeability to pure solvent (water),
κ	Bulk modulus
$\mathbb{T}^{Kort}$	Korteweg stress due to the ideal interface
$\mathbb{T}^{Max}$	Maxwell stress due to the electric displacement
k_B	Boltzmann constant
T	Absolute Temperature
$\mathrm{DEV}\,[\cdot]$	Deviatoric part of the tensor $\mathrm{DEV}\,[\cdot] = \cdot - 1/3\,\mathrm{tr}(\cdot)$

B

$$\boldsymbol{\xi} = \frac{\partial \psi}{\partial \nabla_0 C} =, \tag{89}$$

$$\mu = \frac{\partial \psi}{\partial C} - \nabla_0 \cdot \boldsymbol{\xi} + pv, \tag{90}$$

$$\mathbb{S} = \frac{\partial \psi}{\partial \mathbb{F}} + \frac{\partial \psi}{\partial \mathbb{F}_e}\mathbb{F}_v^{-T} - pJ\mathbb{F}^{-T} \tag{91}$$

C Energy Dissipation.

Combining Equation (50) and (52), and imposing that condition (23) is satisfied, we can characterise the viscous flow by the following relation:

$$\mathbb{L}_v = L_{vv} T^{-1} \left[\mathbb{F}_e^T \frac{\partial \psi}{\partial \mathbb{F}_e} - p_v \mathbb{I} \right] \overset{(*)}{=} \frac{G_2^A}{\eta^A} \mathrm{DEV}\left[\mathbb{C}_e\right], \tag{92}$$

where η^A represent the viscosity of the material and the equality $(*)$ follows from Equation (32):

$$\eta^A tr(\mathbb{L}_v) = tr\left(\mathbb{F}_e^T \frac{\partial \psi}{\partial \mathbb{F}_e} \right) - 3p_v = 0 \Longrightarrow p_v = \frac{tr\left(\mathbb{F}_e^T \frac{\partial \psi}{\partial \mathbb{F}_e} \right)}{3}. \tag{93}$$

Using Equation (42), we obtain:

$$\mathbb{L}_v = \frac{G_2^A}{\eta^A} \mathrm{DEV}[\mathbb{C}_e] = \frac{\mathrm{DEV}[\mathbb{C}_e]}{2\tau_R}. \tag{94}$$

If we now consider the left elastic Cauchy Green tensor $\mathbb{B}_e = \mathbb{F}_e \mathbb{F}_e^T$, we can relate its time derivative to $\mathbb{L}_v$:

$$\begin{aligned} \dot{\mathbb{B}}_e &= \mathbb{L}\mathbb{B}_e + \mathbb{B}_e \mathbb{L}^T - 2\mathbb{F}_e d_v \mathbb{F}_e^T \\ &= \mathbb{L}\mathbb{B}_e + \mathbb{B}_e \mathbb{L}^T - \frac{1}{\tau_R} \mathbb{F}_e \left[\mathbb{C}_e - \frac{1}{3} tr(\mathbb{B}_e) \mathbb{I} \right] \mathbb{F}_e^T \\ &= \mathbb{L}\mathbb{B}_e + \mathbb{B}_e \mathbb{L}^T - \frac{1}{\tau_R} \mathbb{B}_e \underbrace{\left[\mathbb{B}_e - \frac{1}{3} tr(\mathbb{B}_e) \mathbb{I} \right]}_{\mathrm{DEV}[\mathbb{B}_e]}. \end{aligned} \tag{95}$$

For what concern the dissipation due to transport phenomena, the forces ς_m is dependent on the deformation. For this reason, it is more suitable to move from the Lagrangian to the Eulerian coordinates. Using the can rewrite the flux as $\mathbf{j}_m = c_m(\mathbf{v}_m - \mathbf{v}_n) = c_m \bar{\mathbf{v}}_m$, where $\mathbf{v}_m$ is the velocity of the m-th component in the current configuration, $\mathbf{v}_n$ is the velocity of the network also in the current configuration and $\bar{\mathbf{v}}_m$ is the relative velocity of the m-th component with respect to the network.

In the framework of linear non-equilibrium thermodynamics, the transport dissipation function is given by:

$$-c_j \nabla \mu_j = \sum_b L_{jb} \bar{\mathbf{v}}_j = \sum_{i \neq j} f_{ji} \left(\bar{\mathbf{v}}_i - \bar{\mathbf{v}}_j \right) + f_{js} (\bar{\mathbf{v}}_s - \bar{\mathbf{v}}_j) + f_{jn} \bar{\mathbf{v}}_j, \tag{96}$$

$$-c_s \nabla \mu_s = \sum_i f_{si} \left(\bar{\mathbf{v}}_i - \bar{\mathbf{v}}_s \right) + f_{sn} \bar{\mathbf{v}}_s, \tag{97}$$

where f_{mi} and h_{mn} are the drag coefficients related to the interaction between fluid constituents and the polymer network respectively. Based on the Onsanger's reciprocal relation we have that:

$$f_{mb} = f_{bm}. \tag{98}$$

Common assumption in the study of mixture theory is that the solute-solute drag can be neglected so that $f_{ij} = 0$ for $i, j = 1, \dots, N$ [47,**?**]. The remaining drag coefficient are instead defined by:

$$f_{sn} = \frac{1}{k}, \quad f_{js} = \frac{k_B T c_j}{D_j^0}, \quad f_{js} + f_{jn} = \frac{k_B T c_j}{D_j}, \tag{99}$$

where k is the hydraulic permeability of the solvent in the network, D_j^0 is the diffusion coefficient of the solute in pure solution, while D_j is the diffusion coefficient in the gel.

Using (96)-(99), the relative velocities are of the form:

$$\bar{\mathbf{v}}_s = -KJ \left(\nabla \mu_s + \sum_i \frac{D_i}{D_i^0} \frac{C_i}{C_s} \nabla \mu_i \right), \tag{100}$$

$$\bar{\mathbf{v}}_j = -\frac{D_j}{k_B T} \nabla \mu_j + \frac{D_j}{D_j^0} \bar{\mathbf{v}}_s, \tag{101}$$

and the coefficient K is defined as:

$$\frac{1}{K} = \frac{J}{c_s k} + \sum_i \frac{k_B T}{\phi_w} \left(1 - \frac{D_i}{D_i^0} \right) \frac{C_i}{D_i^0}. \tag{102}$$

D Model B: Separating the Volumetric Deformation.

The derivation of the governing equation for the second model proposed follow the same steps as model A, with few changes. From the point of view of conservation laws (Section 4.1), these are still valid as they do not depend on the specific kinetics model chosen. As discussed in Section 4.2, we use multiplicative decomposition to isolate the different contribution to the strain:

$$\mathbb{F} = \bar{\mathbb{F}} \mathbb{F}_{vol} = J^{1/3} \bar{\mathbb{F}}_e \bar{\mathbb{F}}_v, \tag{103}$$

where we have used the fact that $\mathbb{F}_{vol} = J^{1/3} \mathbb{I}$, with $J = \det \mathbb{F}$. Where both $\bar{\mathbb{F}}_e$ and $\bar{\mathbb{F}}_v$ needs to preserve the ECM volume. Analogously to Equation (23), this can be ensured by imposing the following condition:

$$\det \bar{\mathbb{F}}_v = 1. \tag{104}$$

In this case it is easier to express the kinematics of the ECM in terms $\mathbb{L} = \dot{\mathbb{F}} \mathbb{F}^{-1}$, instead of $\dot{\mathbb{F}}$ and $\bar{\mathbb{L}}_v = \dot{\bar{\mathbb{F}}}_v \bar{\mathbb{F}}_v^{-1}$. When we look at the free energy, we now have three decouple mechanical variables that can contribute to it J for the first spring, $\bar{\mathbb{F}}$ and $\bar{\mathbb{F}}_e$ on due to the springs in branch **A** and **B** respectively. Consequently, Equation (30) will now be of the form:

$$\psi = \psi(J, \bar{\mathbb{F}}_e, \bar{\mathbb{F}}, C_s, C_i, \nabla_0 C_s, \mathbf{H}). \tag{105}$$

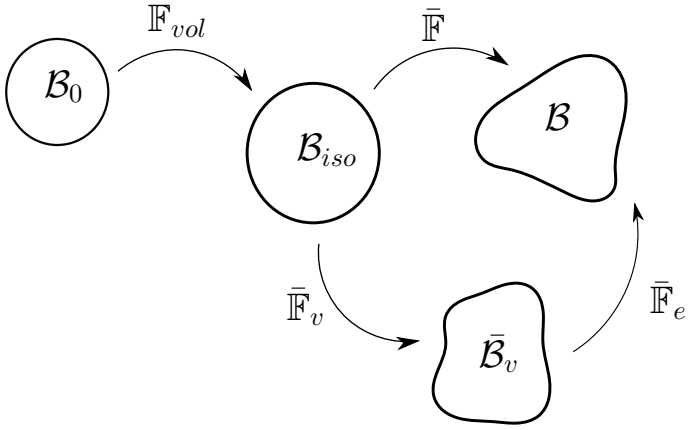

Fig. 12: Multiplicative decomposition of Model B

If we differentiate J, $\bar{\mathbb{F}}$ and $\bar{\mathbb{F}}_e$, we can reduce the number of variables expressing them in terms of $\mathbb{L}$ and $\bar{\mathbb{L}}_v$:

$$\dot{J} = J(\mathbb{I} : \mathbb{L}), \tag{106}$$

$$\dot{\bar{\mathbb{F}}} = J^{-1/3}\mathbb{L}\mathbb{F} - \frac{1}{3}J^{-1/3}(\mathbb{I} : \mathbb{L})\mathbb{F} \tag{107}$$

$$\dot{\bar{\mathbb{F}}}_e = \mathrm{DEV}[\mathbb{L}]\bar{\mathbb{F}}_e - \bar{\mathbb{F}}_e\bar{\mathbb{L}}_v. \tag{108}$$

If we now combine Equations (105)-(108) with the energy inequality, what we obtain is:

$$\begin{aligned}
&\left(\frac{\partial\psi}{\partial\nabla_0 C_s} - \boldsymbol{\xi}\right)\cdot\nabla_0\dot{C}_s + \left(\frac{\partial\psi}{\partial C_s} - \mu_s - \nabla_0\cdot\boldsymbol{\xi} + pv\right)\dot{C}_s \\
&\qquad + \sum_i \left(\frac{\partial\psi}{\partial C_i} + e\Phi z_i - \mu_i\right)\dot{C}_i + \left(\frac{\partial\psi}{\partial\mathbf{H}} - \mathbf{E}\right)\cdot\dot{\mathbf{H}} \\
&+ \left(\mathrm{DEV}\left[J^{-1/3}\frac{\partial\psi}{\partial\bar{\mathbb{F}}}\mathbb{F}^T + \frac{\partial\psi}{\partial\bar{\mathbb{F}}_e}\bar{\mathbb{F}}_e^T\right] - \mathbb{S}\mathbb{F}^T + J\left(\frac{\partial\psi}{\partial J} - p\right)\mathbb{I}\right) : \mathbb{L} \\
&\qquad + \sum_m \nabla_0\,\mu_m\cdot\mathbf{J}_m - \bar{\mathbb{F}}_e^T\frac{\partial\psi}{\partial\bar{\mathbb{F}}_e} : \bar{\mathbb{L}}_v \le 0.
\end{aligned} \tag{109}$$

Finally we need to update the constitutive laws for the strain free energy ψ_6, which, similarly to the case discussed in Section , can be decompose as the sum of contributions from each spring in Figure **??**(b):

$$\psi_6 = \psi_1(\bar{\mathbb{F}}) + \psi_2(\bar{\mathbb{F}}_e) + \psi_{vol}(J). \tag{110}$$

Again we assume the ECM to behave as an hyperplastic material:

$$\psi_1(\bar{\mathbb{F}}) = \frac{G_1^B}{2}\left(\bar{\mathbb{F}} : \bar{\mathbb{F}} - 3\right), \tag{111}$$

$$\psi_2(\bar{\mathbb{F}}_e) = \frac{G_2^B}{2}\left(\bar{\mathbb{F}}_e : \bar{\mathbb{F}}_e - 3\right). \tag{112}$$

For the volumetric contribution we consider as before a logarithmic term:

$$\psi_{vol}(J) = \frac{\kappa}{2}\ln J^2. \tag{113}$$

ALTERNATIVE:

$$\psi_{vol}(J) = \frac{G_{vol}}{2}\left[3(J^{2/3} - 1) - \ln J^2\right]. \tag{114}$$

The above volumetric constitutive assumption is one of the most common in modelling hyper-elastic material. However, as shown in [37], this has several limitation in the regime of large deformation, which highlights the need of study more realistic form which can capture the more complex behaviour of real material. From this point of view, being able to decouple the volumetric deformation as in model B allows to investigate this aspect alone [REPHRASE].

When looking at the entropy production, Equation (43) still holds simply by replacing $\mathbb{L}_v$ with $\bar{\mathbb{L}}_v$. Using the same argument as in Section (4.5), we are left with the following system of equations:

$$\boldsymbol{\xi} = \gamma J\, \mathbb{B}^{-1}\, \nabla_0\, C_s, \tag{115}$$

$$\begin{aligned}\mu_s = pv + \mu_s^0 - \gamma J \nabla^2 C_s + kT\Bigg[&\ln\frac{C_s v}{1+C_s v} + \frac{1}{1+C_s v} \\ &+ \frac{\chi}{(1+C_s v)^2} - \sum_i \frac{C_i}{C_s}\Bigg],\end{aligned} \tag{116}$$

$$\mu_i = \mu_i^0 + e\Phi z_i + kT\ln\frac{C_i}{C_s}, \tag{117}$$

$$\mathbf{E} = \frac{1}{\epsilon J}\mathbb{F}^T\mathbb{F}\,\mathbf{H} \tag{118}$$

$$\begin{aligned}\mathbb{T} = &\left(\frac{\kappa}{1+C_s v_s} - p\right)\mathbb{I} + \frac{G_1^B}{1+C_s v}\mathrm{DEV}[\bar{\mathbb{B}}] + \frac{G_2^B}{1+C_s v}\mathrm{DEV}[\bar{\mathbb{B}}_e] \\ &+\gamma\left[\frac{1}{2}|\nabla C_s|^2\mathbb{I} - \nabla C_s \otimes \nabla C_s\right] + \epsilon\left[\frac{1}{2}|\nabla\Phi|^2\mathbb{I} - \nabla\Phi\otimes\nabla\Phi\right],\end{aligned} \tag{119}$$

coupled to the governing equations:

$$\mathbf{j}_s = -Kc_s\left(c_s\nabla\mu_s + \sum_i \frac{D_i}{D_i^0}c_i\nabla\mu_i\right), \tag{120}$$

$$\mathbf{j}_i = -\frac{D_i}{k_BT}c_i\nabla\mu_i + \frac{D_i}{D_i^0}\frac{c_i}{c_s}\mathbf{j}_s, \tag{121}$$

$$\dot{\bar{\mathbb{B}}}_e = \bar{\mathbb{B}}_e\mathbb{L}^T + \mathbb{L}\bar{\mathbb{B}}_e - \frac{2}{3}tr(\mathbb{L})\bar{\mathbb{B}}_e - \frac{1}{\tau_R}\bar{\mathbb{B}}_e\mathrm{DEV}\left[\bar{\mathbb{B}}_e\right] \tag{122}$$

References

1. Anand, L.: A thermo-mechanically-coupled theory accounting for hydrogen diffusion and large elastic–viscoplastic deformations of metals. International Journal of Solids and Structures **48**(6), 962 – 971 (2011)
2. Benfenati, F., Beretta, G.P.: Ergodicity, Maximum Entropy Production, and Steepest Entropy Ascent in the Proofs of Onsager's Reciprocal Relations. Journal of Non Equilibrium Thermodynamics **43**, 101–110 (Apr 2018)
3. Beretta, G.P.: The fourth law of thermodynamics: steepest entropy ascent. arXiv preprint arXiv:1908.05768 (2019)
4. Bergström, J., Boyce, M.: Constitutive modeling of the large strain time-dependent behavior of elastomers. Journal of the Mechanics and Physics of Solids **46**(5), 931 – 954 (1998)
5. Bertet, C., Sulak, L., Lecuit, T.: Myosin-dependent junction remodelling controls planar cell intercalation and axis elongation. Nature **429**, 667–71 (07 2004)
6. Biot, M.A.: General theory of three-dimensional consolidation. Journal of Applied Physics **12**(2), 155–164 (1941)
7. Boyce, M.C., Arruda, E.M.: Constitutive models of rubber elasticity: A review. Rubber Chemistry and Technology **73**(3), 504–523 (2000)
8. Buenger, D., Topuz, F., Groll, J.: Hydrogels in sensing applications. Progress in Polymer Science **37**(12), 1678 – 1719 (2012)
9. Butcher, D., Alliston, T., Weaver, V.: A tense situation: forcing tumour progression. nat rev cancer 9: 108-122. Nature reviews. Cancer **9**, 108–22 (03 2009)
10. Caccavo, D., Cascone, S., Lamberti, G., Barba, A.A.: Hydrogels: experimental characterization and mathematical modelling of their mechanical and diffusive behaviour. Chem. Soc. Rev. **47**, 2357–2373 (2018)
11. Caccavo, D., Vietri, A., Lamberti, G., Barba, A.A., Larsson, A.: Modeling the mechanics and the transport phenomena in hydrogels. In: Manca, D. (ed.) Quantitative Systems Pharmacology, Computer Aided Chemical Engineering, vol. 42, chap. 12, pp. 357 – 383. Elsevier (2018)
12. Chaudhuri, O.: Viscoelastic hydrogels for 3d cell culture. Biomater. Sci. **5**, 1480–1490 (2017)
13. Cohen Stuart, M., Huck, W., Genzer, J., Müller, M., Ober, C., Stamm, M., Sukhorukov, G., Szleifer, I., Tsukruk, V., Urban, M., Winnik, F., Zauscher, S., Luzinov, I., Minko, S.: Emerging applications of stimuli-responsive polymer materials. Nature materials **9**, 101–13 (2010)
14. Deligkaris, K., Tadele, T.S., Olthuis, W., Van den Berg, A.: Hydrogel-based devices for biomedical applications. Sensors and Actuators B: Chemical **147**, 765–774 (2010)
15. Doi, M.: Soft Matter Physics. OUP Oxford (2013)
16. Dolega, M., Delarue, M., Ingremeau, F., Prost, J., Delon, A., Cappello, G.: Cell-like pressure sensors reveal increase of mechanical stress towards the core of multicellular spheroids under compression. Nature Communications **8**, 14056 (2017)
17. Drozdov, A.: Swelling of ph-responsive cationic gels: Constitutive modeling and structure–property relations. International Journal of Solids and Structures **64-65**, 176 – 190 (2015)
18. Drozdov, A.D., deClaville Christiansen, J., Sanporean, C.G.: Inhomogeneous swelling of ph-responsive gels. International Journal of Solids and Structures **87**, 11 – 25 (2016)

19. Flory, P.J.: Thermodynamics of high polymer solutions. The Journal of Chemical Physics **10**(1), 51–61 (1942)
20. Flory, P.: Principles of Polymer Chemistry. Baker lectures 1948, Cornell University Press (1953)
21. Garcia-Gonzalez, D., Jerusalem, A.: Energy based mechano-electrophysiological model of cns damage at the tissue scale. Journal of the Mechanics and Physics of Solids **125**, 22 – 37 (2019)
22. Garcia-Gonzalez, D.: Magneto-visco-hyperelasticity for hard-magnetic soft materials: theory and numerical applications. Smart Materials and Structures **28**(8), 085020 (jul 2019)
23. Gurtin, M.E.: Generalized ginzburg-landau and cahn-hilliard equations based on a microforce balance. Physica D: Nonlinear Phenomena **92**(3), 178 – 192 (1996)
24. Hennessy, M.G., Münch, A., Wagner, B.: Surface induced phase separation of a swelling hydrogel (2018), preprint on webpage `http://www.wias-berlin.de/preprint/2562/wias_preprints_2562.pdf`
25. Hong, W.: Continuum Models of Stimuli-responsive Gels, pp. 165–196. Springer Berlin Heidelberg, Berlin, Heidelberg (2012)
26. Hong, W., Wang, X.: A phase-field model for systems with coupled large deformation and mass transport. Journal of the Mechanics and Physics of Solids **61**(6), 1281 – 1294 (2013)
27. Hu, Y., Suo, Z.: Viscoelasticity and poroelasticity in elastomeric gels. Acta Mechanica Solida Sinica **25**(5), 441 – 458 (2012)
28. Huggins, M.L.: Some properties of solutions of long-chain compounds. The Journal of Physical Chemistry **46**(1), 151–158 (1942)
29. Kondepudi, D., Prigogine, I.: Modern Thermodynamics: From Heat Engines to Dissipative Structures. CourseSmart, John Wiley & Sons (2014)
30. Kröner, E.: Allgemeine Kontinuumstheorie der Versetzungen und Eigenspannungen. Archive for Rational Mechanics and Analysis **4**, 273–334 (1959)
31. Larché, F., Cahn, J.: The interactions of composition and stress in crystalline solids. Acta Metallurgica **33**(3), 331 – 357 (1985)
32. Lebon, G., Jou, D., José, C.V.: Understanding Non-Equilibrium Thermodynamics. Springer-Verlag Berlin Heidelberg (01 2008)
33. Levental, I., Georges, P.C., Janmey, P.A.: Soft biological materials and their impact on cell function. Soft Matter **3**, 299–306 (2007)
34. Li, J., Mooney, D.: Designing hydrogels for controlled drug delivery. Nature Reviews Materials **1**, 16071 (2016)
35. Lubarda, V.A.: Constitutive theories based on the multiplicative decomposition of deformation gradient: Thermoelasticity, elastoplasticity, and biomechanics . Applied Mechanics Reviews **57**(2), 95–108 (04 2004)
36. Marsland, R., England, J.: Limits of predictions in thermodynamic systems: a review. Reports on Progress in Physics **81**(1) (2017)
37. Moerman, K.M., Fereidoonnezhad, B., McGarry, P.: Novel hyperelastic models for large volumetric deformations (Feb 2019)
38. Netti, P.A., Berk, D.A., Swartz, M.A., Grodzinsky, A.J., Jain, R.K.: Role of extracellular matrix assembly in interstitial transport in solid tumors. Cancer Research **60**(9), 2497–2503 (2000)
39. N'Guyen, T., Lejeunes, S., Eyheramendy, D., Boukamel, A.: A thermodynamical framework for the thermo-chemo-mechanical couplings in soft materials at finite strain. Mechanics of Materials **95**, 158 – 171 (2016)
40. Onsager, L.: Reciprocal relations in irreversible processes. i. Phys. Rev. **37**, 405–426 (Feb 1931)

41. Paszek, M.J., Zahir, N., Johnson, K.R., Lakins, J.N., Rozenberg, G.I., Gefen, A., Reinhart-King, C.A., Margulies, S.S., Dembo, M., Boettiger, D., Hammer, D.A., Weaver, V.M.: Tensional homeostasis and the malignant phenotype. Cancer Cell **8**(3), 241 – 254 (2005)
42. Prigogine, I.: Introduction to thermodynamics of irreversible processes. Interscience Publishers (1968)
43. Rauzi, M., Vérant, P., Lecuit, T., Lenne, P.F.: Nature and anisotropy of cortical forces orienting drosophila tissue morphogenesis. Nature Cell Biology **10**, 1401–1410 (2008)
44. Sun, D.N., Gu, W.Y., Guo, X.E., Lai, W.M., Mow, V.C.: A mixed finite element formulation of triphasic mechano-electrochemical theory for charged, hydrated biological soft tissues. International Journal for Numerical Methods in Engineering **45**(10), 1375–1402 (1999)
45. Wang, X., Hong, W.: A visco-poroelastic theory for polymeric gels. Proceedings of the Royal Society A: Mathematical, Physical and Engineering Sciences **468**(2148), 3824–3841 (2012). https://doi.org/10.1098/rspa.2012.0385
46. Xue, S.L., Li, B., Feng, X.Q., Gao, H.: Biochemomechanical poroelastic theory of avascular tumor growth. Journal of the Mechanics and Physics of Solids **94**, 409 – 432 (2016)
47. Xue, S.L., Li, B., Feng, X.Q., Gao, H.: A non-equilibrium thermodynamic model for tumor extracellular matrix with enzymatic degradation. Journal of the Mechanics and Physics of Solids **104**, 32 – 56 (2017)
48. Xue, S.L., Lin, S.Z., Li, B., Feng, X.Q.: A nonlinear poroelastic theory of solid tumors with glycosaminoglycan swelling. Journal of Theoretical Biology **433**, 49 – 56 (2017)
49. Yu, Y., Landis, C.M., Huang, R.: Salt-Induced Swelling and Volume Phase Transition of Polyelectrolyte Gels. Journal of Applied Mechanics **84**(5) (03 2017)